GEOPHYSICAL RESEARCH LETTERS, VOL. 31, L24111, doi:10.1029/2004GL021165, 2004

Tidal perturbations and variability in the mesopause region over Fort Collins, CO (41N, 105W): Continuous multi-day temperature and wind lidar observations

C. Y. She, Tao Li, Richard L. Collins,[1] Tao Yuan, Bifford P. Williams, Takuya D. Kawahara,[2] Joe D. Vance, Phil Acott, and David A. Krueger
Physics Department, Colorado State University, Fort Collins, Colorado, USA

Han-Li Liu and Maura E. Hagan
High Altitude Observatory, National Center for Atmospheric Research, Boulder, Colorado, USA

Received 30 July 2004; revised 6 October 2004; accepted 26 October 2004; published 31 December 2004.

[1] An unusually long data set was acquired at the sodium lidar facility at Colorado State University (41N, 105W), between Sep 18 and Oct 01, 2003, including a 9-day continuous observation. This time is long enough to average out the perturbations of gravity waves and short-period planetary waves. As such, it can be used to define tidal-period perturbations in temperature and horizontal wind. Assuming the sodium mixing ratio is a constant of motion, the observed tidal-period oscillation in sodium density follows that of vertical wind. Thus, the data set defines tidal-period perturbations of temperature and wind vector. The observed amplitudes and phases were compared to Global Scale Wave Model predictions (both GSWM00 and GSWM02). We found excellent agreement in diurnal phases and reasonable agreement in semidiurnal phases. However, GSWM02 overestimates diurnal amplitudes and both model versions underestimate observed semidiurnal amplitudes. Since the data period is long enough for the study of planetary waves and of tidal variability, we perform spectral analysis of the data, revealing a strong quasi 3-day wave in meridional wind, a 14 hour perturbation in zonal wind, and both 14-hour and 10-hour periods in meridional wind, likely the result of nonlinear interactions. The observed semidiurnal amplitudes are much larger than the corresponding diurnal amplitudes above 85 km, and over a few days the diurnal and semidiurnal amplitudes vary by factors of 2–3. Causes for the observed tidal variability in terms of planetary wave modulation and tide-gravity wave interaction are explored qualitatively. *INDEX TERMS:* 3360 Meteorology and Atmospheric Dynamics: Remote sensing; 3334 Meteorology and Atmospheric Dynamics: Middle atmosphere dynamics (0341, 0342); 3384 Meteorology and Atmospheric Dynamics: Waves and tides. **Citation:** She, C. Y., et al. (2004), Tidal perturbations and variability in the mesopause region over Fort Collins, CO (41N, 105W): Continuous multi-day temperature and wind lidar observations, *Geophys. Res. Lett.*, *31*, L24111, doi:10.1029/2004GL021165.

1. Introduction

[2] In May 2002, the Colorado State University sodium lidar [*Arnold and She*, 2003] was upgraded to allow two-beam measurements during both day and night. This upgraded system now supports simultaneous measurements of mesopause region Na density, temperature, zonal wind and meridional wind over full diurnal cycles under clear sky conditions. During the second half of Sep 2003, fair weather prevailed in northern Colorado, and an unusually long data set of 14-day duration was acquired between Sep 18 and Oct 01 including a 9-day continuous observation. The length of this lidar observation exceeds that of other middle atmosphere lidar observations to-date, and is similar to that of radar campaigns [*Thayaparan et al.*, 1995]. Multi-day observations of this type allow studies where the shorter-period planetary waves (PW) and gravity waves (GW) can be averaged out and the analysis can focus on the recurrent tidal wind and temperature perturbations. In addition, since above 85 km sodium atoms may be used as a neutral tracer in the mesopause region, i.e., ignoring chemical effects [*Xu and Smith*, 2003], sodium density perturbations track those of vertical wind. This allows the use of measured diurnal and semidiurnal perturbations in sodium density and in temperature to deduce vertical wind perturbations of the same periods [*Batista et al.*, 1985]. Therefore, one purpose of this paper is to determine diurnal and semidiurnal perturbations in the mesopause region temperature, zonal, meridional and vertical wind components. The results are compared to the corresponding tidal prediction from Global Scale Wave Models [*Hagan and Forbes*, 2002]. Since the data set is long enough, we also conduct a tidal variability study, and examine PW and GW perturbations as well as their nonlinear interactions with tidal waves.

2. Data Set and Tidal-Period Analysis

[3] The lidar signals consist of photon profiles of Na fluorescence from east and north beams, each pointing 30° from zenith. The signal is integrated every 2 minutes and saved to produce a photo-count profile from each beam. For tidal analysis, we first sum the photo-count profiles in each hour and vertically smooth with a Hanning window of 2 km, FWHM, for data acquired at night and 4 km under sunlit conditions. The resulting profiles are analyzed to

[1] Permanently at Geophysical Institute, University of Alaska, Fairbanks, Alaska, USA.
[2] On leave from Faculty of Engineering, Shinshu University, Nagano, Japan.

0094-8276/04/2004GL021165

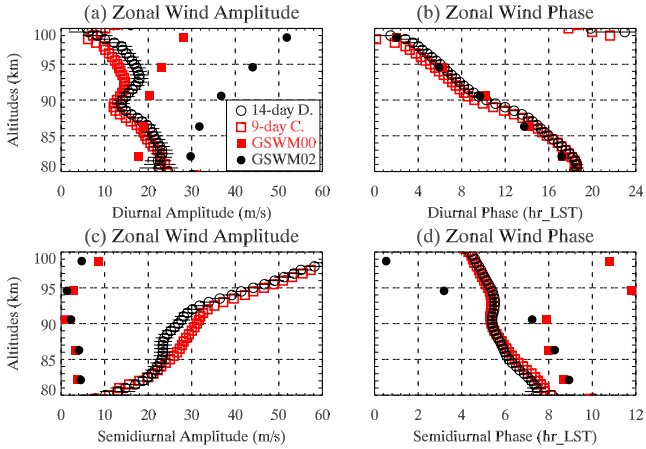

Figure 1. Diurnal and semidiurnal September zonal wind tides.

deduce line-of-sight wind and temperature for each beam. Assuming the hourly mean vertical wind is negligible, hourly mean profiles of zonal wind can be determined from the observation of the east-beam, of meridional wind from the north-beam, and of temperature from the average of the two beams. The measurement precision for hourly temperature and winds under nighttime fair sky conditions were estimated to be, respectively, 0.5 K and 1.5 m/s at the Na peak (92 km), and 5 K and 15 m/s at the edges (81 and 107 km) of the sodium layer. Due to the use of the Faraday filter [*Chen et al.*, 1993], the measurement uncertainty under sunlit condition would be at least 1.5 times larger depending on sky background.

[4] We form two data sets from these hourly profiles: (1) a 9-day continuous (9-day-C) set between 04UT, day 264 and 22UT, day 272, and (2) a 14-day duration (14-day-D) set, which in addition to the 9-day-C, consists of a 33-hr observation (from 16UT, day 261 to 01UT, day 263) prior to, and a 24-hr observation (from 02UT, day 274 to 01UT, day 275) after it. The time series of both data sets, over sampled at 0.5 km intervals, are linearly fit at each altitude to a constant plus sum of perturbations with diurnal, semidiurnal, terdiurnal and quatradiurnal periods [*She*, 2004] for this study. For spectral analysis and variability study, the 9-day-C data set is binned in 30min intervals in daytime and 15min at night with 2 km resolution.

3. Diurnal and Semidiurnal Amplitudes and Phases

[5] The presence of oscillations with diurnal and semidiurnal periods can be seen easily from contour plots of hourly mean profiles of mesopause region temperature, zonal and meridional winds (not shown) without analysis. Both data sets were harmonically analyzed, yielding the best-fit profiles of diurnal and semidiurnal tidal amplitudes and phases for all four fields. These profiles with error bars were plotted along with the predictions of both GSWM00 and GSWM02 for comparison. The difference between two model versions lies in the fact that GSWM02 includes both nonmigrating and migrating effects while GSWM00 is migrating only. To save space, we show these profiles between 80 and 100 km only for zonal wind in Figure 1. While there is negligible difference between the two GSWM predictions in diurnal phases, the GSWM02 diurnal amplitude typically is a factor of two bigger. The two data sets, 9-day-C and 14-day-D, yield the same tidal amplitudes and phases. Data over a total of 14 days should give an average tidal characteristics of the month in question, leading to a meaningful comparison with the model tide. When observation and model predictions are compared, the agreement in diurnal phase is excellent for all four fields. The GSWM02 overestimates the diurnal amplitude, while the GSWM00 fairs much better. For semidiurnal comparison, we see reasonable agreement in phases, with GSWM predictions underestimating the observed amplitude by an order of magnitude. The agreement between observation and the GSWM00 predictions suggests that the migrating tide dominates observed diurnal-period perturbations. The marginal agreement in semidiurnal phase along with much larger observed amplitudes suggests that either strong local sources exist or the model missed significant global sources with semidiurnal periods in September. Radar wind measurements from globally distributed stations for a summer campaign in 1999 [*Pancheva et al.*, 2002] and from nearby Platteville, CO with two years of observation [*Mason et al.*, 2003] also found agreement with GSWM00 prediction in diurnal tides and discrepancy in semidiurnal tides.

[6] Since the tidal amplitudes often are different above and below 90 km, while the phases could be either similar or different, we report tidal characteristics by tabulating the amplitudes and phases at 86 km and 96 km in Table 1 for observation (O) and GSWM predictions (G). Notice, the observed semidiurnal amplitudes are greater than the observed diurnal amplitudes for all fields. Other than one exception in zonal wind semidiurnal phase at 96 km, the GSWM00 and GSWM02 diurnal and semidiurnal phases, and semidiurnal amplitudes are nearly the same; thus, only one value is given in Table 1. GSWM02 diurnal amplitudes are much bigger than those of GSWM00; the latter is in better agreement with observation. We note comparable observed wind amplitudes between zonal and meridional components, for both DA(O) and SA(O). From Table 1, SP(O) of meridional wind leads that of zonal wind, which in turn leads that of temperature, each by ~90 degree,

Table 1. Diurnal and Semidiurnal Amplitudes (DA, SA); Phase (DP, SP)

Fields (km)	DA (O)[a]	DA (G)[b]	DP (O)[c]	DP (G)	SA (O)	SA (G)	SP (O)	SP (G)[d]
T(86)	3.0	3.5/7	4.0	9.8	9.0	1.0	11	12
T(96)	7.2	7.5/13	23.8	24	12	3.1	8.9	7.0
u(86)	20	19/32	15	14	23	4.0	6.1	8.1
u(96)	15	25/46	4.9	5	47	2.8	5.1	11
v(86)	15	20/33	9.3	10	24	5.0	3.3	4.8
v(96)	5.6	18/36	21.5	23	50	4.5	2.3	8.9
w(86)	7.5	5.0/–	14.9	14	20	2.2	1.9	1.6
w(96)	3.7	5.4/–	4.9	7	10	4.6	9.9	10

[a]Units are K, m/s and cm/s for T, u or v, and w, respectively.
[b]Diurnal amplitude for GSWM (00/02) models different, both given.
[c]Phase indicates local time of max value, has unit of hr.
[d]SP (semidiurnal phases) roughly the same for both GSWM models, except for zonal wind at 96 km, with 11.4 and 2.5 hr for 00 and 02.

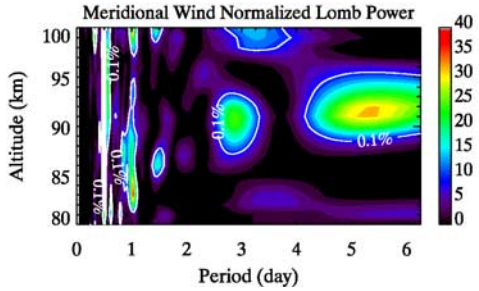

Figure 2. Normalized Lomb power contours of meridional wind based on the 9-day-C data set are shown with the contour corresponding to 0.1% probability resulting from random noise marked. Lomb power of 20 corresponds to 1×10^{-5}% probability.

consistent with the polarization relations of upward and westward propagating waves.

4. Spectral Analysis: Lomb Periodogram

[7] Lomb Periodograms can accept unevenly spaced time series; they are an effective way to reveal the frequency contents in a data set including tidal periods. Monte Carlo simulation with the same temporal structure may be used to assign a percent probability that a given Lomb power would be present in random noise. Using the 9-day-C data set with 2 km and 15min (30min) resolution for nighttime (daytime) observation, the normalized Lomb periodogram for meridional wind is shown in Figure 2. As expected the diurnal and semidiurnal components are very strong at all altitudes between 80 and 100 km. However, the terdiurnal component also is significant. In addition, we see a prominent quasi 5-day period between 89 and 95 km, a quasi 3-day period between 87 and 94 km, and a 1.5-day period between 85 and 88 km, which likely represent planetary waves. While they appear to be overpowered by the semidiurnal tide, there exists power at 20-hr, 14-hr and 10-hr periods, respectively, between 85 and 89, 90 and 100 km and 87 and 90 km, which are likely the results of nonlinear interactions, similar to those identified in our April data [*She et al.*, 2003]. We tabulate the observed periods with significant Lomb power (having less than 0.1% probability of being due to random noise) for temperature, zonal and meridional winds in Table 2, along with a preliminary indication of their possible sources. However, the frequency relationship between the primary and secondary waves alone is not enough to unequivocally ascribe the nonlinear interaction,

Table 2. Significant Non-Tidal-Period Oscillations

Dynamic Field	Period (hours)	Range (km)	Sources (Primary Periods)
Temp.	102	85–88	quasi 4-day
Zonal wind	14	87–100	nonlinear (12h, 3d)
	17	89–93	nonlinear (12h,1.5d)
	20	85–89	nonlinear (1d, 5d)
	36	84–88, 93–99	quasi 1.5-day
Meridional wind	10	87–90	nonlinear (12h, 3d)
	14	90–100	nonlinear (12h, 3d)
	20	85–89	nonlinear (1d, 5d)
	36	85–88	quasi 1.5-day
	70	87–94	quasi 3-day
	130	89–95	quasi 5-day

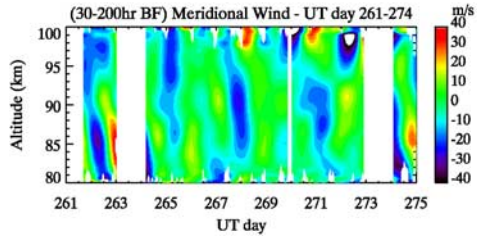

Figure 3. Filtered meridional wind contours by a band-pass filter with sharp cutoffs at 30 and 200 hours.

and the vertical wavenumber of the secondary wave should be determined. Since this will depend not only on the primary wavenumbers but also on the depth of the interaction region as well as the specific mode of the secondary wave, a more detailed study is obviously necessary for their full understanding. Thus, while Table 2 suggests the richness of this data set, the explanation put forth is merely plausible and not definitive. To reveal the coherence of the observed planetary waves, contours of meridional wind in 1hr intervals of the 14-day-D data set, filtered by a band-pass filter with sharp cutoffs at 30 and 200 hours, are shown in Figure 3. A wind minimum with a period of ~3 days is clearly seen to progress downward at ~1.3 km/day. Phase progression with ~1.5-day period (yellow maxima) can also be seen below 90 km. In addition, maxima near days 262, 267 and 272 at 90 km suggests the presence of a quasi 5-day perturbation.

5. Tidal Variability

[8] Using the 9-day continuous data set with 2 km and 15–30min resolution, we have performed running tidal analyses using individual 24-hour continuous data sets, centered at each hour. In this manner, we can investigate the variability of diurnal-means, tidal amplitudes and phases. The variability (in absolute values) is smallest in diurnal-means and largest in semidiurnal amplitudes, consistent with considerable nonlinear interactions associated with 12hr period, see Table 2. Only diurnal and semidiurnal amplitude of temperature and zonal wind are shown in Figure 4. These show not only day-to-day variability but

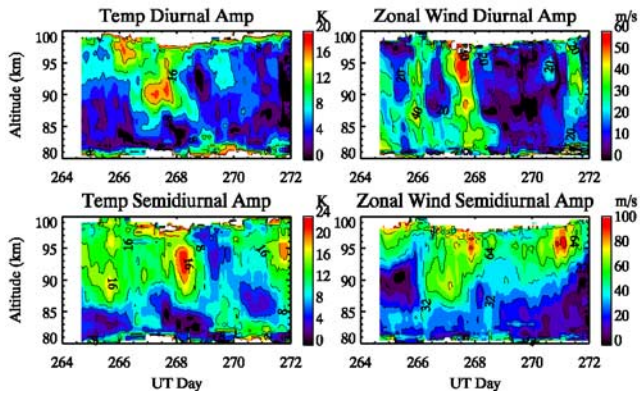

Figure 4. Variability in diurnal and semidiurnal amplitudes of temperature (left) and zonal wind (right) during 9-day observation. Notice scale differences.

also a large increase in amplitudes between noon, day 266 (Sep 23) and noon, day 268, with the maximum increase in diurnal amplitude occurring before that in semidiurnal amplitude by about half a day. We note that though the variability in diurnal phases is larger in comparison, the altitude-dependent semidiurnal phases (not shown) are robust against interactions. In these 9 days, they remain constant within two hours at each altitude.

[9] The variability of the apparent tidal amplitudes and phases could be caused by interactions with planetary waves on global scales [*Hagan and Roble*, 2001] or interactions with gravity waves, or combination of both. As shown in Figures 2 and 3, perturbations with periods of 1.5-day, 3-day, and quasi 5-day are present during these 9 days, which may be associated with planetary waves. Previous studies [*Meyer and Forbes*, 1997] demonstrated that planetary waves with a period near 6.5-days may indeed peak around equinox.

[10] The local apparent tidal amplitudes and phases may also change due to interactions with GW [*Waterscheid*, 1981; *Fritts and Vincent*, 1987]. The tides modulate the atmospheric stability and thus GW breaking, and the wave breaking leads to changes of local mean wind and temperature. The temperature inversions thus formed can be strong and are characterized by near adiabatic lapse rates at the top side due to turbulent mixing in the wave breaking region [*Liu and Hagan*, 1998]. At the same time, momentum deposition due to wave breaking changes the zonal wind. Temperature inversions with adiabatic or near adiabatic lapse rates were indeed observed on days 267 and 268. In Figure 5a we show three 15-min mean temperature profiles between 7 and 8UT Day 267, showing ~25 K inversions near 90 km. The corresponding zonal wind changes from −90 m/s at 86 km to 90 m/s at 96 km are shown in Figure 5b. On day 267, temperature inversions around 90 km are seen between 4 and 11UT while zonal wind profiles similar to those of Figure 5b were observed with downward phase progression between 5 and 12UT. From observations at a single station, however, it is difficult to sort out the relative contributions of PW and GW to the observed large zonal wind changes, or indeed, the extent of tide-GW interactions.

6. Conclusion

[11] An unprecedented multi-day observation was completed with the upgraded CSU sodium lidar between Sep 18 and October 01, 2003, including a 9-day continuous observation. Harmonic analysis of observed profiles of mesopause region temperature, zonal and meridional winds, as well as Na density led to the determination of amplitudes and phases of diurnal and semidiurnal perturbations in all four dynamical fields, i.e., temperature and the wind vector. The observed results were compared to GSWM predictions. We find excellent (good) agreement between predictions and observation in diurnal (semidiurnal) phases. While agreement is also very good between GSWM00 and observed diurnal amplitudes, the GSWM02 overestimates the observed diurnal amplitude by about a factor of 2, and both predictions underestimate the observed semidiurnal amplitudes in September by an order of magnitude.

[12] Spectral analysis of temperature, zonal and meridional winds led to the identification of quasi 1.5-day, 3-day and 5-day waves. These are likely planetary waves, though their origins and characteristics are not presently known. In addition to the tidal periods, the spectral analysis also revealed periods of ~20, ~14 and ~10 hours, which are likely products of nonlinear interactions between tides and PW. Considerable day-to-day variations in diurnal and semidiurnal tidal amplitudes were observed along with a large increase by factors of 2–3 in diurnal and semidiurnal amplitudes in days 266–268.

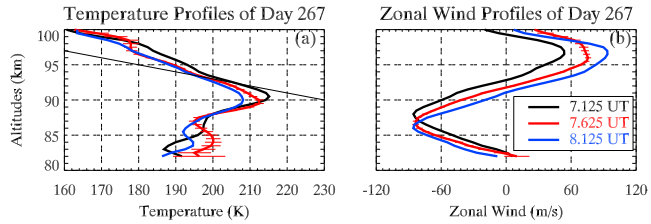

Figure 5. Three 15-min mean profiles of temperature with the thin line indicating the adiabatic lapse rate, (a), and zonal wind (b), between 7hr and 8hr, UT, Day 267.

[13] The possible causes for the observed large tidal variability were discussed in relations to PW modulation and GW interactions, revealing the complexity of tide-GW interaction. We have demonstrated that substantial information on MLT dynamics may be obtained from a comprehensive long-period data set, probing temperature and wind fields simultaneously. We also note the need for correlative modeling studies as well as spaceborne and ground-based observations at selected longitudes and latitudes for global perspective.

[14] **Acknowledgments.** This work is supported in part by grants from National Aeronautics and Space Administration, NAG5-10076 and NAG5-13567, and from National Science Foundation, ATM-0003171 and ATM-0335127, and ATM-0137555. The National Center for Atmospheric Research is supported by the National Science Foundation.

References

Arnold, K. S., and C. Y. She (2003), Metal fluorescence lidar (light detection and ranging) and the middle atmosphere, *Cont. Phys.*, *44*, 35–49.

Batista, P. P., B. R. Clemsha, D. M. Simonich, and V. W. J. H. Kirchhoff (1985), Tidal oscillations in the atmospheric layer, *J. Geophys. Res.*, *90*, 3881–3888.

Chen, H., C. Y. She, and E. Korevaar (1993), Na Vapor dispersive Faraday filter, *Opt. Lett.*, *18*, 1019–1021.

Fritts, D. C., and R. A. Vincent (1987), Mesospheric momentum flux studies at Adelaide, Australia: Observations and a gravity wave-tide interaction model, *J. Atmos. Sci.*, *44*, 605–619.

Hagan, M. E., and J. M. Forbes (2002), Migrating and nonmigrating semidiurnal tides in the middle and upper atmosphere excited by tropospheric latent heat release, *J. Geophys. Res.*, *107*(D24), 4754, doi:10.1029/2001JD001236.

Hagan, M. E., and R. G. Roble (2001), Modeling diurnal tidal variability with the National Center for Atmospheric Research thermosphere-ionosphere-mesosphere-energetics and dynamic general circulation model, *J. Geophys. Res.*, *106*, 24,869–24,882.

Liu, H.-L., and M. E. Hagan (1998), Local heating/cooling of the mesosphere due to gravity wave and tidal coupling, *Geophys. Res. Lett.*, *25*, 2941–2944.

Mason, A. H., et al. (2003), Ionospheric and dynamical characteristics of the mesosphere-lower thermosphere region over Platteville (40°N, 105°W) and comparisons with the region over Saskatoon (52°N, 107°W), *J. Geophys. Res.*, *108*(D13), 4398, doi:10.1029/2002JD002835.

Meyer, C. K., and J. M. Forbes (1997), A 6.5-day westward propagating planetary wave: Origin and characteristics, *J. Geophys. Res.*, *102*, 26,173–26,178.

Pancheva, D., et al. (2002), Global-scale tidal structure in the mesosphere and lower thermosphere during PSMOS campaign of June–August 1999

and comparison with the global-scale wave model, *J. Atmos. Sol. Terr. Phys.*, *64*, 1011–1035.

She, C.-Y. (2004), Initial full-diurnal-cycle mesopause region lidar observations: Diurnal-means and tidal perturbations of temperature and winds over Fort Collins, CO (41N, 105W), PSMOS 2002, *J. Atmos. Sol. Terr. Phys.*, *66*, 663–674.

She, C.-Y., J. Sherman, T. Yuan et al. (2003), The first 80-hour continuous lidar campaign for simultaneous observation of mesopause region temperature and wind, *Geophys. Res. Lett.*, *30*(6), 1319, doi:10.1029/2002GL016412.

Thayaparan, T., W. K. Hocking, and J. MacDougall (1995), Observational evidence of tidal/gravity wave interaction using the UWO 2 MHz radar, *Geophys. Res. Lett.*, *22*, 373–376.

Waterscheid, R. L. (1981), Inertio-gravity wave induced accelerations of mean flow having an imposed periodic component: Implications on tidal observations in the meteor region, *J. Geophys. Res.*, *86*, 9698–9706.

Xu, J., and A. K. Smith (2003), Perturbations of the sodium layer: Controlled by chemistry or dynamics, *Geophys. Res. Lett.*, *30*(20), 2056, doi:10.1029/2003GL018040.

P. Acott, R. L. Collins, T. D. Kawahara, D. A. Krueger, T. Li, C. Y. She, J. D. Vance, B. P. Williams, and T. Yuan, Physics Department, Colorado State University, Fort Collins, CO 80526, USA. (joeshe@lamar.colostate.edu)

M. E. Hagan and H.-L. Liu, High Altitude Observatory, National Center for Atmospheric Research, P.O. Box 3000, Boulder, CO 80307, USA.